NAVAL POSTGRADUATE SCHOOL
Monterey, California

THESIS

THE EFFECTS OF ISOTHERMAL DEFORMATION AND ANNEALING ON THE MICROSTRUCTURE OF NICKEL-ALUMINUM-BRONZE PROPELLER MATERIAL

by

William Adolph Nabach

June 2003

Thesis Advisor: Terry McNelley

Approved for public release: distribution is unlimited

THIS PAGE INTENTIONALLY LEFT BLANK

REPORT DOCUMENTATION PAGE			Form Approved OMB No. 0704-0188
Public reporting burden for this collection of information is estimated to average 1 hour per response, including the time for reviewing instruction, searching existing data sources, gathering and maintaining the data needed, and completing and reviewing the collection of information. Send comments regarding this burden estimate or any other aspect of this collection of information, including suggestions for reducing this burden, to Washington headquarters Services, Directorate for Information Operations and Reports, 1215 Jefferson Davis Highway, Suite 1204, Arlington, VA 22202-4302, and to the Office of Management and Budget, Paperwork Reduction Project (0704-0188) Washington DC 20503.			
1. AGENCY USE ONLY ***(Leave blank)***	**2. REPORT DATE** June, 2003	**3. REPORT TYPE AND DATES COVERED** Master's Thesis	
4. TITLE AND SUBTITLE: Miscrostructural effects of Isothermal Deformation and Annealing on Nickel-Aluminum-Bronze Materials			**5. FUNDING NUMBERS**
6. AUTHOR(S) William Adolph Nabach			
7. PERFORMING ORGANIZATION NAME(S) AND ADDRESS(ES) Naval Postgraduate School Monterey, CA 93943-5000			**8. PERFORMING ORGANIZATION REPORT NUMBER**
9. SPONSORING /MONITORING AGENCY NAME(S) AND ADDRESS(ES) N/A			**10. SPONSORING/MONITORING AGENCY REPORT NUMBER**
11. SUPPLEMENTARY NOTES The views expressed in this thesis are those of the author and do not reflect the official policy or position of the Department of Defense or the U.S. Government.			
12a. DISTRIBUTION / AVAILABILITY STATEMENT Approved for public release: distribution is unlimited			**12b. DISTRIBUTION CODE**

13. ABSTRACT ***(maximum 200 words)***

This thesis is a study of annealing and deformation characteristics of cast Nickel-Aluminum Bronze (NAB) in relation to Friction Stir Processing (FSP) of this material. Cast NAB is widely utilized by the U.S. Navy as material used in the production of propellers for surface vessel and submarines. FSP is a novel method of deformation processing that is conducted by use of a rotating tool that is forced onto the surface of a material under load such that sliding and sticking friction result in a combination of frictional and adiabatic heating due to plastic deformation. A stirring effect results in the formation of a zone of severe shear deformation and local temperatures approaching 90% of the melting temperature. FSP results in local homogenization of the cast microstructure and conversion of it to a wrought condition, but also in steep strain, strain rate and temperature gradients. In this thesis microstructures achieved through controlled isothermal deformation and annealing processes will be compared with microstructures resulting from FSP. The use of Friction Stir Processing is envisioned as a way to improve the surface characteristics of the material through localized microstructural modification. Studies of warm rolling, channel die compression and various annealing schedules were completed.

14. SUBJECT TERMS Friction Stir Processing, Nickel-Aluminum-Bronze, NAB, Isothermal Deformation, Annealing, Optical Microscopy, Scanning Electron Microscopy, Naval Propellers, Surface Treatment, Thermomechanically-Affected Zone, Shear Deformation. Channel Die Compression, Lamellar tearing, Grain Growth, Homogenization of Microstructure	**15. NUMBER OF PAGES** 63
	16. PRICE CODE

17. SECURITY CLASSIFICATION OF REPORT	**18. SECURITY CLASSIFICATION OF THIS PAGE**	**19. SECURITY CLASSIFICATION OF ABSTRACT**	**20. LIMITATION OF ABSTRACT**
Unclassified	Unclassified	Unclassified	UL

NSN 7540-01-280-5500 Standard Form 298 (Rev. 2-89)
Prescribed by ANSI Std. 239-18

THIS PAGE INTENTIONALLY LEFT BLANK

Approved for public release: distribution is unlimited

THE EFFECTS OF ISOTHERMAL DEFORMATION AND ANNEALING ON THE MICROSTRUCTURE OF NICKEL-ALUMINUM-BRONZE PROPELLER MATERIAL

William A. Nabach
Lieutenant, United States Coast Guard
B.S. Marine Transportation, U.S. Merchant Marine Academy, 1998

Submitted in partial fulfillment of the
requirements for the degree of

**MASTER OF SCIENCE IN
MECHANICAL ENGINEERING**

from the

**NAVAL POSTGRADUATE SCHOOL
June 2003**

Author: William A. Nabach

Approved by: Terry R. McNelley
Thesis Advisor

Young W. Kwon
Chairman, Department of Mechanical Engineering

THIS PAGE INTENTIONALLY LEFT BLANK

ABSTRACT

This thesis is a study of annealing and isothermal deformation characteristics of cast Nickel-Aluminum Bronze (NAB) in relation to Friction Stir Processing (FSP) of this material. Cast NAB is widely utilized by the U.S. Navy in the production of propellers for surface vessel and submarines. FSP is a novel method of deformation processing that is conducted by use of a rotating tool that is forced onto the surface of a material under load such that sliding and sticking friction result in a combination of frictional heating and adiabatic heating due to plastic deformation. A stirring effect results in the formation of a zone of severe shear deformation and local temperatures approaching 90% of the melting temperature. FSP results in local homogenization of the cast microstructure and conversion of it to a wrought condition in the absence of macroscopic shape change, but also in steep strain, strain rate and temperature gradients. In this thesis microstructures achieved through controlled isothermal deformation and annealing processes are recorded and analyzed. Studies of warm rolling, channel die compression and various annealing schedules were completed.

THIS PAGE INTENTIONALLY LEFT BLANK

TABLE OF CONTENTS

THIS PAGE INTENTIONALLY LEFT BLANK

LIST OF FIGURES

THIS PAGE INTENTIONALLY LEFT BLANK

LIST OF TABLES

THIS PAGE INTENTIONALLY LEFT BLANK

ACKNOWLEDGMENTS

The author would like to thank the Defense Advanced Research Projects Agency (DARPA) for funding and support of this research; the Naval Surface Warfare Center (Carderock Division) for the NAB material and technical support; and Murray W. Mahoney at the Rockwell Science Center for his support, presentations and also for allowing the FSP group to witness FSP'ing in action.

The author would like to thank Professor Terry McNelley for providing the necessary direction and redirection for this research project.

The author would also like thank Charles Roe (NSWC-Carderock), Asunta Cuevas, K. Oishi, Chanman Park and Doug Swisher for sharing their knowledge of all things microscopy, NAB, and everything else… thanks.

Special thanks to the rest of the FSP thesis crew (C.F. Walton and K. Faires) for all of their help and support through this process.

Last but not least, the author would like to thank friends and family for lending their support and motivation.

THIS PAGE INTENTIONALLY LEFT BLANK

I. INTRODUCTION

A. NICKEL-ALUMINUM BRONZE

Nickel-aluminum bronze (NAB) is a copper based alloy with aluminum, nickel and iron alloying additions that is used extensively for marine applications. NAB exhibits excellent corrosion resistance as well as good strength making it the material of choice for applications including propellers for United States Navy surface and sub-surface platforms. In addition to its overall strength and corrosion resistance, NAB also demonstrates other important characteristics. These include [Ref. 1] i) good wearabiltiy and low friction coefficients; ii) high damping capacity; iii) exceptional fatigue resistance; iv) good fracture toughness at both elevated and lower temperatures; and v) moderate tensile strength through a wide temperature range. Aside from the propeller applications, valve parts, fittings, pumps, etc. for both freshwater and seawater service are also fabricated from NAB.

The Navy casts propellers using an NAB alloy designated UNS C95800, commonly referred to as alpha nickel aluminum bronze or propeller bronze [Ref. 2]. NAB propellers are sand-cast in accordance with the ASTM B148 specification for aluminum bronze castings [Ref. 3]. The procedures designated by the ASTM B148 specification give a complicated microstructure [Ref. 4]. Because cooling rates in large castings are difficult to control, varied cooling rates also give rise to non-uniform NAB microstructures and reduced material properties and performance. In addition, gas evolution during solidification and cooling results in porosity, further degrading material strength and corrosion resistance. [Ref 5]

With respect to propellers, the coarse microstructure and porosity developed in casting contribute to an overall reduction in material performance. It is necessary that casting methods of propellers produce the best possible quality of microstructure since a high strength is needed to withstand the forces on the propeller as it engages the water. In addition, weaker microstructures inherent in cast propellers show greater susceptibility to corrosion and fatigue, especially in an aggressive environment such as seawater. [Ref.

6] This, as well as, cavitation due to propeller motion through the water, greatly reduces the service life. A surface hardening technique that strengthens surface layers of the propeller by improving microstructure and by the removal of casting defects would help resolve many of these difficulties.

Techniques to control and repair defects in cast NAB propellers include welding, which produces a non-equilibrium microstructures and introduces thermal stresses that further degrade corrosion resistance of the alloy. To combat this annealing is used on welded sections, but this yields only a marginal improvement. [Ref. 7] The best circumstance would be a process that creates a fine microstructure in the surface layers while maintaining the ductility of the material. This will ultimately lead to propellers with higher strength and increased cavitation resistance. Friction-stir processing represents a technology which my be applied to NAB propellers to obtain the aforementioned attributes.

B. FRICTION STIR PROCESSING

FSP is a microstructural refinement process adapted from friction-stir welding [Ref. 8]. The technique uses a rotating tool that is pressed onto and traversed across the material surface to produce extreme plastic deformation as the tool "stirs" the material underneath it. The localized, severe plastic deformation and heating of the material homogenizes the microstructure and thereby improves material properties. The FSP tool consists of a cylindrical "shoulder" with a pin projection at its end that is in contact with the material as it is being processed. The shoulder interacts with the surface of the processed material to forge material softened by the intense deformation and adiabatic heating produced during FSP. What remains is a region of intense shear deformation with a fine-grained microstructure.

It is important to note that, although the intense plastic deformation may transfer material from one side of the tool to the other, FSP is a solid-state process, never melting the processed material. Studies on the effects of friction-stir processing on NAB as well as aluminum and magnesium alloys [Ref. 9-11] reveal that FSP improves material

strength as well as ductility, which is desired for propeller application. A direct possibility for this process is not only to repair casting defects, but could radically influence future propeller design. However, a better understanding of the temperature and strain rates and strain states attained is needed in order to better model the process and find the optimum processing parameters.

C. OBJECTIVES:

Friction Stir Processing comprises two main features: adiabatic heating and severe plastic deformation. Furthermore, the process involves steep gradients in temperature, strain and strain rate. In this thesis the goal was to separately examine the effects of heating and deformation separately, and in the absence of gradients, and record the respective microstructural effects of each. For this thesis isothermal rolling, isothermal channel die compression, and static annealing were employed with NAB material samples from a large, coarse-grained casting.

1. ANNEALING

An annealing study was designed to simulate the range of temperatures that has been modeled and calculated for the FSP'ing of NAB. A peak temperature above 850°C has been calculated. The schedule that was developed for the annealing study reflects a full range of temperatures from about 380°C (0.5 T_m) to 900°C (0.9 T_m). The resultant microstructures are recorded and compared to ascertain the effects of temperature upon a coarse NAB microstructure.

2. ROLLING

The rolling study was undertaken as a conventional means through which large amounts of deformation could be imparted to NAB samples under isothermal conditions over the same temperature range that was utilized for the

annealing treatment. The resultant microstructures, phase changes and deformation shapes would be used to attempt to calculate out strain rates and strain states encountered in FSP.

3. CHANNEL DIE COMPRESSION:

As with the rolling study, Channel Die Compression was envisioned as a conventional process by which NAB samples could be deformed to high degrees of strain. A series of isothermal Channel Die Compression runs could be used to augment the rolling data over the same range of temperatures.

The overall objective of this thesis was to create a catalog of the resultant microstructures from two or three congruent isothermal processes conducted over the same range of temperatures.

II. BACKGROUND

The composition and phase transformations of NAB will be reviewed in this Chapter. Also, a more in-depth explanation of FSP concentrating on the development of shear through plastic deformation will be considered. In addition, the chapter will attest to the incomparable effects of FSP on NAB microstructure, as well as discuss how known shear textures developed in NAB compare with those developed in other commercial alloys such as aluminum and magnesium alloys.

A. DEVELOPMENT OF NICKEL ALUMINUM BRONZE

Nickel-aluminum bronze is a quaternary alloy based on the copper-aluminum system. Composition ranges, including the specific composition used in this research can be found in Table 1. Cu-Al binary alloys exhibit the following phases and behaviors: 1) alloys containing less than 7% aluminum solidify as a single-phase alpha (α) solid solution, with a face-centered cubic (FCC) crystal structure and, upon cooling to room temperature, retain this alpha phase; 2) alloys with greater than 9.4 wt.% Al solidify as a single-phase beta (β) solid solution, which has a body centered cubic (BCC) crystal structure. Upon slow cooling, this β phase forms the α phase, and remnant β transforms by a eutectoid reaction into α + gamma (γ). The Al-rich γ phase has a lower electrochemical potential than the Cu rich α phase. This results in the preferential corrosion or de-aluminization of the alloy. [Ref. 6] Alloying may be employed with Cu-Al alloys to retard the formation of γ.

The additions of nickel and iron into the Cu-Al alloy system effectively extend the alpha phase while precluding the formation of the γ phase even as the Al content is increased [Ref. 6, 12]. This may be seen in the three ternary equilibrium phase diagrams, for a nominal temperature of 500ºC, which are shown in Figure 2.1. The Ni and Fe additions result in the formation of intermetallic kappa (κ) phases that replace the γ, and also confer improved material properties in NAB.

	Cu	Al	Ni	Fe	Mn	Si	Pb
min-max	(min) 79.0	8.5-9.5	4.0-5.0	3.5-4.5	0.8-1.5	(max) 0.10	(max) 0.03
Nominal	81	9	5	4	1	-	-
Alloy	81.2	9.39	4.29	3.67	1.20	0.05	<0.005

Table 1. Composition (wt.%) of UNS C95800 NAB Material (Metals Hnbk, 9th Ed.) Bottom row represents composition of alloy used in this study.

Alloys containing more than 3 wt. % Fe display a reduction in elevated temperature grain growth in addition to a reduced grain size and a reduced solidification range. Higher Fe content (3 - 5 wt. %) increases strength and the retention of this strength at higher temperatures. A nominal 4 wt. % Fe has been commonly accepted as the optimum Fe content, greatly improving wear resistance, abrasion resistance, and fatigue endurance. [Ref. 12]

The addition of Ni (0-5 wt.%) increases strength and provides a grain refining effect like Fe. [Ref. 12] The Ni also impedes the formation of the β phase upon cooling and increases hardness. However, it is important to note that alloys with a nickel content less than that of iron are susceptible to second-phase corrosion attack in seawater. A nominal content of 5 wt. % Ni and 4wt. % Fe is deemed ideal for maximum corrosion resistance.

As previously mentioned, the additions of Ni and Fe in nickel-aluminum bronze allow for an increased aluminum content. It has been determined that Al content ranging from 8.8 – 10 wt. % results in good corrosion resistance with increased hardness and strength. [Ref. 12] However, further increases in Al content also results in a decrease in elongation due to increased formation of the lamellar κ_{iii} phase, which resides along the grain boundaries. [Ref. 12] The optimum combination of properties appears to be

achieved using an Al content of 9.5 wt. % (Table 1). The material of this research conforms to the composition limits for NAB.

B. PHASES IN CAST NICKEL ALUMINUM BRONZE

For a nominal 9 wt. % Al content as-cast nickel-aluminum bronze first solidifies as BCC β, as for binary Cu-Al alloys. Upon further cooling the β decomposes to give the four distinct phases of NAB: an FCC α matrix and three kappa phases designated κ_{ii}, κ_{iii}, and κ_{iv}. These κ phases have been classified according to both their individual morphologies as observed through optical microscopy (OM) and on the sequence in which they form from the β phase. [Refs 13-14] The phases will be described in this order. These phases are also identified on the micrograph of as-cast NAB shown in Figure 2.2a.

1. Alpha (α)

The alpha phase is an equilibrium solid solution with a face centered cubic (fcc) crystal structure. It has a lattice parameter a= 3.64 Å. [Ref. 15] Alpha forms beginning at about 1030^{o}C from β and often displays as a Widmanstätten morphology during slow to moderate cooling from the beta phase, which is congruent with the casting of large parts such as propellers. Alpha can occur intergranularly or intragranularly but slower cooled NAB consists of primarily intragranular alpha. [Ref. 16] The α phase can be seen as the light phase in figure 2.2a.

2. Kappa II (κ_{ii})

In the literature there have been four κ phases classified in as-cast NAB. [Ref. 13] This included a Kappa I (κ_i) phase, as well as the κ_{ii}, κ_{iii}, and κ_{iv} phases. The κ_i phase is of the same composition and crystal structure as the κ_{ii}, only larger in size, and found in alloys containing more that 5 wt. % Fe. The κ_{ii} phase is a globular, dendritic (rosette-shaped) phase in NAB alloys. [Refs 15-16] It can range in particle size from 5 to 50 μm and is iron rich with a nominal Fe_3Al composition. It has been determined that

the κ_{ii} phase has a DO_3 crystal structure with a lattice parameter, a, equaling 5.71Å. [Ref 15] The DO_3 structure is defined as an ordered bcc superlattice consisting of eight cells (Figure 2.2b). The β phase begins to form at about 900ºC during cooling, and κ_{ii} often resides at the periphery of α grains or in the lamellar eutectoid region of the microstructure. A Cu-Al phase diagram for 5 wt.% Ni and 4 wt. % Fe is represented in Figure 2.3.

3. Kappa IV (κ_{iv})

Kappa IV is a fine cuboidal, cruciform precipitate, typically 2 μm in size, formed within the α matrix at 860°C. The κ_{iv} particles are of the same Fe_3Al composition and DO_3 crystal structure as the κ_{ii} phase. The lattice parameter (a) for the κ_{iv} phase is 5.77 Å versus the 5.71 Å for κ_{ii}. [Ref. 15]

4. Kappa III (κ_{iii})

Kappa III phase forms fine lamellar particles following the eutectoid decomposition of β and has a nominal NiAl composition. The κ_{iii} has a B2 crystal structure with a lattice parameter, a= 2.88 angstroms (approximately half that of κ_{ii} and κ_{iv}). [Ref. 15, 17] The B_2 structure for NiAl is an ordered CsCl crystal structure, which is hypothesized as forming from κ_{ii} particles that may act as a substrate for κ_{iii} growth [Ref 17]. Forming at around 800°C, κ_{iii} can have a fine lamellar morphology while proeutectoid κ_{iii} has a fine, globular morphology.

The casting response of NAB is variable, resulting in varied phase distributions and material properties within the casting. One reason for this is the slow cooling rates inherent in the casting of large structures (i.e., propellers). The other is difficulty in control of alloying composition in NAB. Casting porosity gives further degradation of material properties. This will ultimately lead to lower material strength and decreased cavitation and corrosion resistances.

Propellers experience severe environmental conditions and stresses throughout their service lives. Cavitation, corrosion, and stresses from routine operation serve to

erode, corrode and weaken propeller surfaces. Therefore the major concern for manufacturing propellers and larger NAB components is to eliminate the inherent defects in casting without significantly altering the fabrication process. This will extend the service life of the parts and reduce overall maintenance costs. Friction-stir processing, which has been shown to drastically improve the material properties of NAB, can accomplish this task.

C. FRICTION STIR PROCESSING

In 1991 The Welding Institute (TWI) developed a new state of the art welding process known as friction-stir welding (FSW) [Ref. 8]. Friction-stir processing (FSP) represents a groundbreaking microstructural refinement process engendered by FSW technology. the "stirring" motion of the tool in FSP, instead of joining two materials as in friction-stir welding, is used to create a more homogenized microstructure with improved material properties.

Friction-stir processing uses a non-consumable tool attached to a modified milling machine. The tool, often fabricated of tool steel, consists of a cylindrical shoulder with a smaller diameter concentric pin at its end. The tool is rotated and plunged into the clamped material (to avoid excessive movement) until the shoulder engages the material surface, as seen in the schematic of Figure 2.4. Once engaged the tool is then traversed across the material surface in a single pass or in multiple passes. The shoulder and length of the pin control the depth of surface treatment penetration. The rotating pin, through mainly sticking friction (there is also some sliding friction), induces plastic deformation and adiabatic heating on a small column of material near the tool center. A larger region of material around the central column is plastically deformed by contact with the rotating shoulder. The shoulder also acts to contain the upward flow of metal that is being physically displaced by the pin, and to forge heated material. Tool shoulder diameter is typically approximately 25 mm, with pin diameter generally between 6 and 10 mm and pin depth ranging from 6 to 12 mm. [Ref. 18] The sticking friction and large plastic

deformations produce adiabatic heating of the material. This heating softens the material but does not melt it. A typical temperature distributions due to tool rotation is seen in Figure 2.5. [Ref. 27] Friction-stir processing is a solid-state process, with the intense plasticity of FSP moving material from one side of the tool and depositing it on the other. Once completed, a processed NAB sample consists of three distinct regions, namely the 1) stir zone/ nugget, 2) the thermo-mechanically affected zone, 3) base metal (Figure 2.6).

The stir zone, or nugget, is the region most highly affected by FSP. It is characterized by intense plastic deformation and a resultant fine-grained, defect free microstructure. The nugget represents the objective of friction-stir processing: a refined microstructure with improved material properties. Grain sizes in the stir zone are refined to perhaps 3 μm. [Ref. 7] Tensile tests of specimens fabricated from the stir zone of NAB revealed a doubling of yield strength coupled with an approximate 66% increase in ultimate tensile strength. (Figure 2.7a) A significant increase in ductility was observed as well. The stir zone and TMAZ exhibit increased hardness compared to base metal as well. (Figure 2.7b) The stir zone in nickel-aluminum bronze may be heterogeneous, comprising fine, equiaxed grains in some regions as well as Widmanstätten structures elsewhere. Beneath the stir zone is a region of less severe plastic deformation and heating effects, identified as the thermo-mechanically affected zone (TMAZ).

The TMAZ exhibits some similarity to a heat-affected zone (HAZ) in conventional fusion welding. However, this region is characterized by plastic deformations (but not as much as the stir zone) coupled with heating effects created by adiabatic heating due to the rotating tool. Therefore, the TMAZ experiences steep strain, strain rate and temperature gradients over a distance of approximately 200 to 400 μm. The grain structure in the TMAZ consists of large grains that have been deformed in shear during FSP. The TMAZ still exhibits improved material properties (due to removal defects) over the parent material.

The base metal embodies the bulk of the material, which remains relatively unaffected by processing except for minor heating effects near the base metal/ TMAZ

interface. Base metal will exhibit a microstructure and material properties dependant upon on the casting conditions. In the casting of propellers, the section thicknesses are so large that cooling of as-cast material to ambient temperature may require days. For this reason, it is expected that as-cast material from such applications will exhibit equilibrium microstructures. Finally, the as-cast NAB material will include casting defects such as porosity.

The microstructure and mechanical properties of FSP'ed NAB material vary throughout the stir zone and TMAZ due to local variations in peak temperature attained, subsequent cooling rate, and due to gradients in strain and strain rate. Interpretation of the effects of FSP on microstructure has been made more complicated because of the simultaneous effects of all of these factors. Thus, it is useful to consider separately the effects of each of the various factors. The effect of temperature alone may be evaluated through isothermal annealing of NAB samples although subsequent cooling rate will also influence resulting microstructures. Deformation alone may be evaluated through isothermal rolling or by means of compression or tension testing.

FSP is an important future method of material processing technology. However before it can be used on a scale beyond experimental, every aspect of the process and its effects on the material require understanding. The motivation for this research derives its basis from this concept. Ultimately it will be desirable to be able to model the deformation process and include in the models the ability to predict microstructures as well as local temperatures, strains and strain rates. With the ability to predict microstructures it should then become possible to predict the properties of as-processed material via simulation methods. Nevertheless, FSP for nickel-aluminum bronze is a viable undertaking, but will require both extensive experimentation and model development prior to industrial implementation.

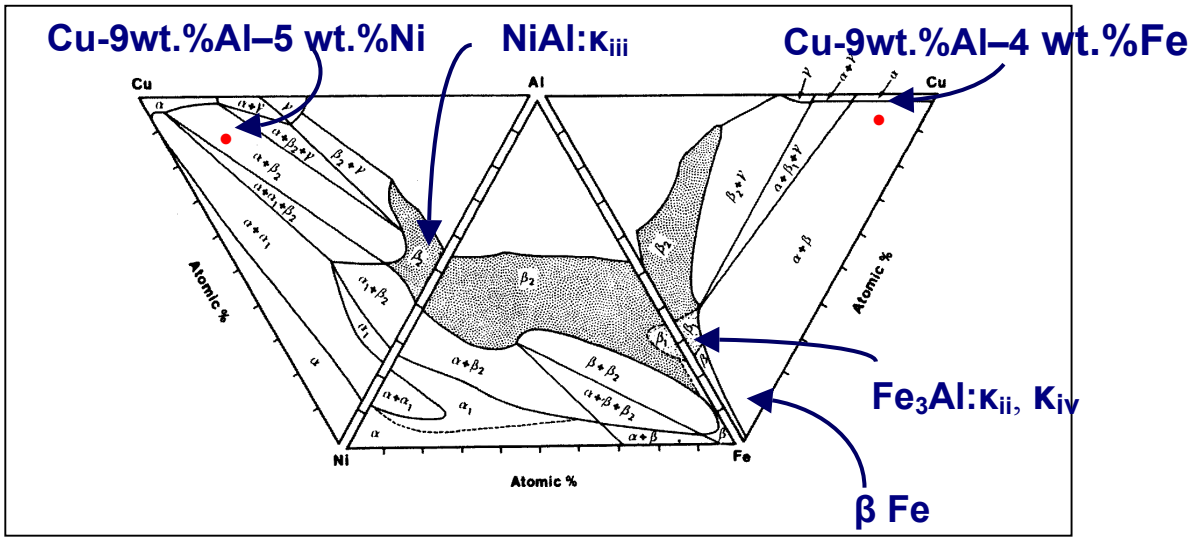

Figure 2.1: Quaternary equilibrium NAB phase diagram. F. Hasan, A. Jahanafrooz, G.W. Lorimer and N. Ridley, Metall. Trans. A., vol. 13A (1982) pp. 1337-45. (*Modified courtesy T. R. McNelley.*) [Ref. 15]

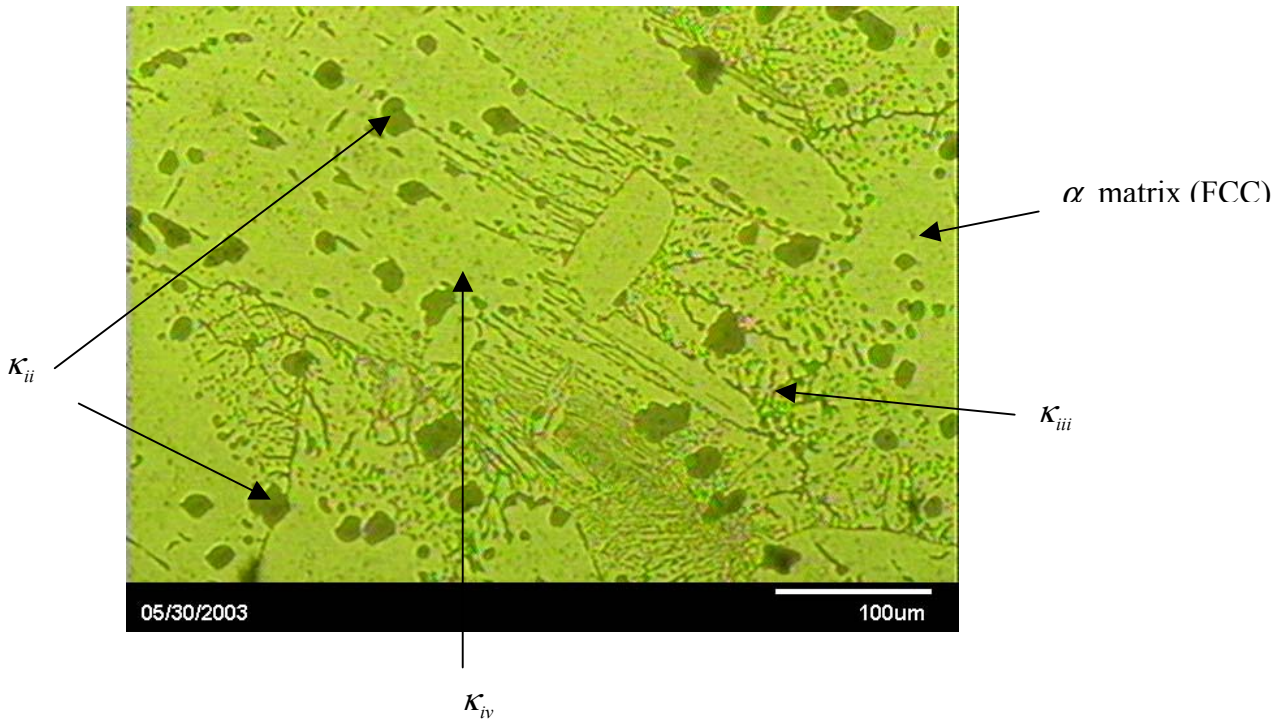

Figure 2.2a: Optical micrograph of 380°C annealed NAB at 370x. κ_{ii} is the globular, dendritic structure, κ_{iv} is the very fine particulate imbedded with in the α matrix (surrounding light green phase), κ_{iii} is the lamellar "finger-like" structure.

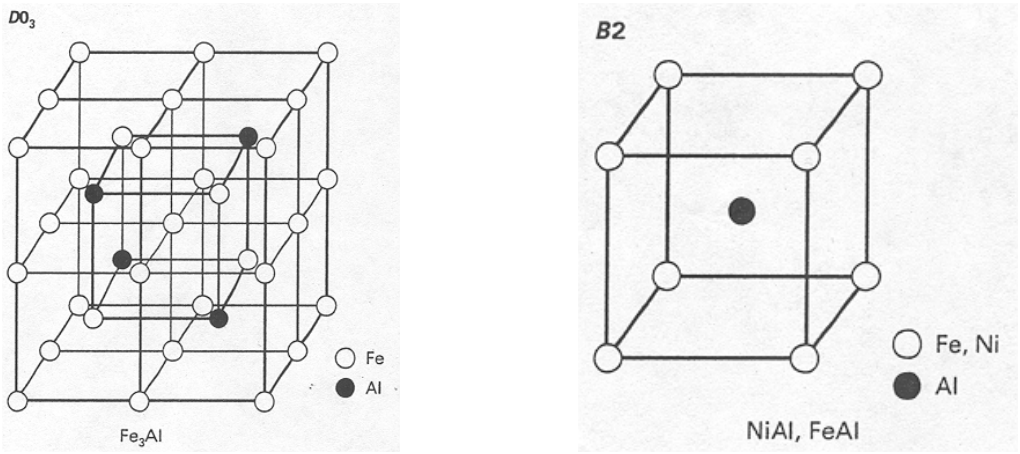

Figure 2.2b: DO3 and B2 crystal structures. κii and κiv have a Fe3Al composition with a D03 crystal structure, while κiii exhibits a NiAl composition with a B2 crystal structure. [Ref. 15]

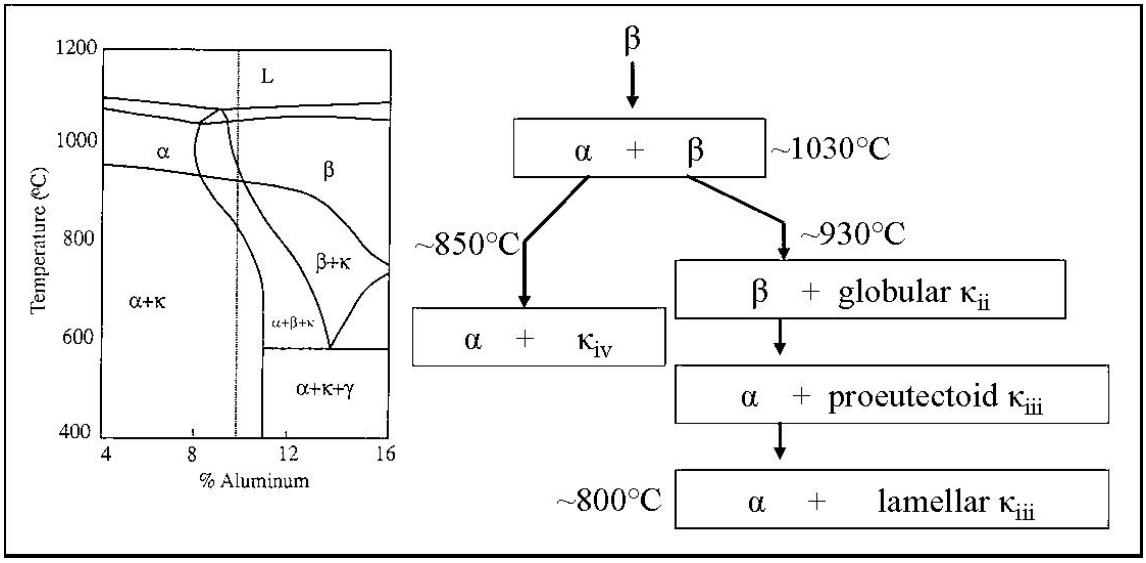

Figure 2.3: NAB phase diagram with corresponding transformation diagram. [Ref 13&21]

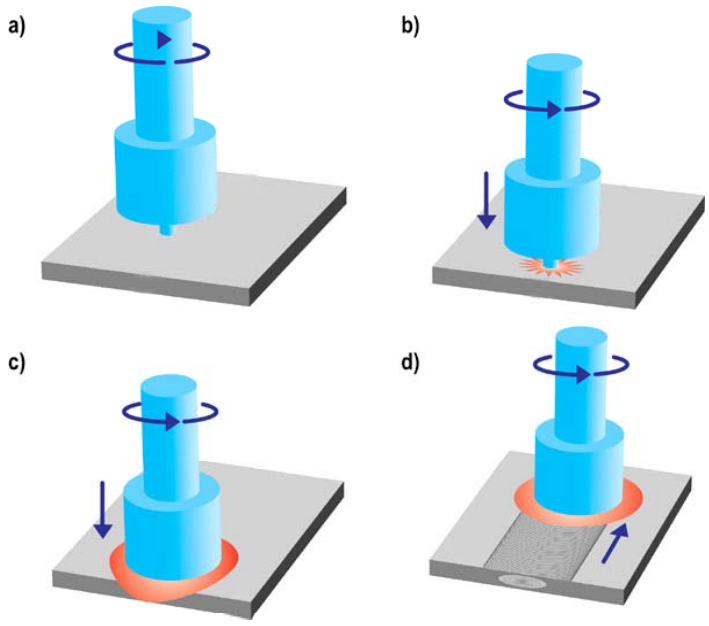

Figure 2.4: Friction Stir Process. A rotating tool a) is plunged into the material surface b). Once engaged up to the shoulder c) the tool is traversed across the material surface d). FSP is not a superficial process, affecting material well below the pin depth. The advancing side is that in which tool rotation and tool translation are in the same direction. On the retreating side tool rotation is opposite tool translation. (Courtesy M. W. Mahoney, RSC).

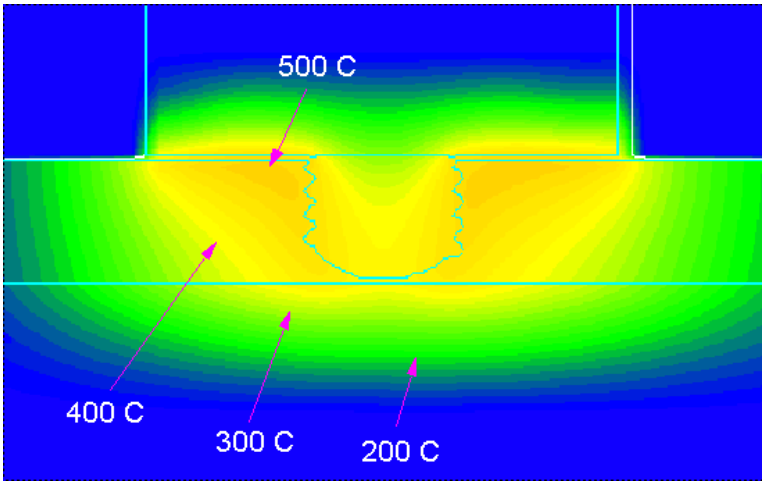

Figure 2.5: Temperature distribution in FSP. Temperatures have been known to reach upwards of 850°C. A. Askari, Boeing INC, Private Communication.

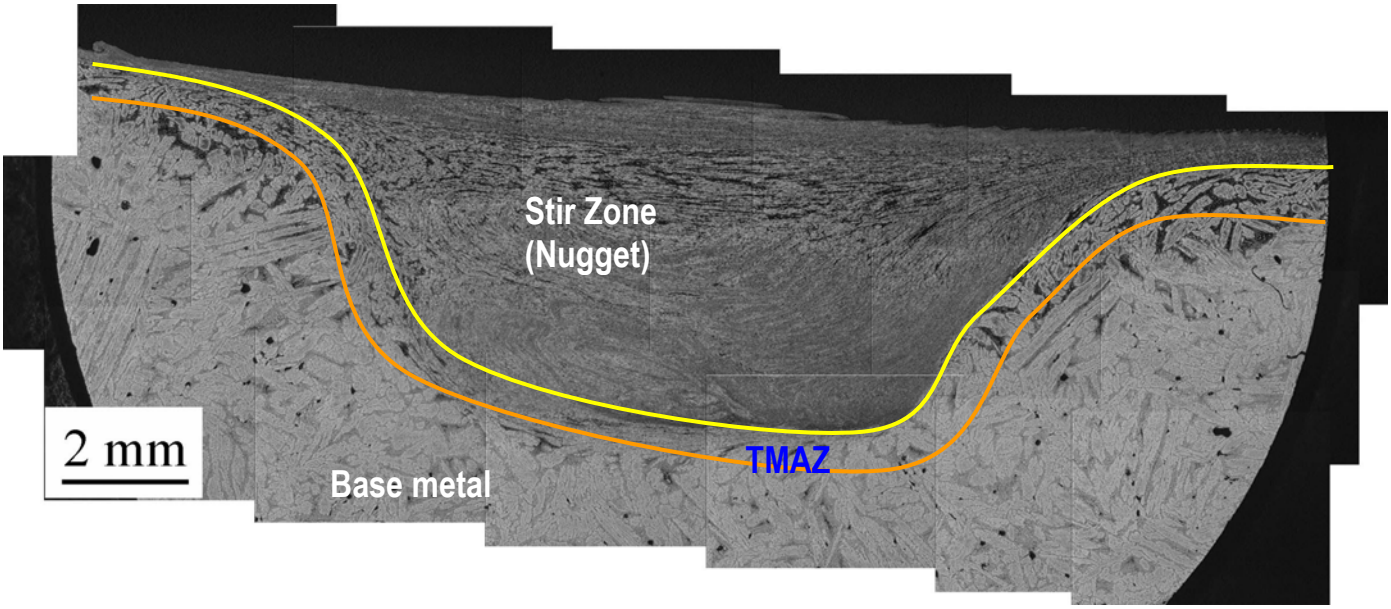

Figure 2.6: Regions resulting from FSP. The stir zone is characterized by extensive plastic deformation as induced by the rotating tool. The TMAZ experiences both large plastic deformations and heating effects. Base metal remains relatively unchanged from the as-cast condition, experiencing minute deformations and heating effects. (*Courtesy K. Oishi, NPS*)

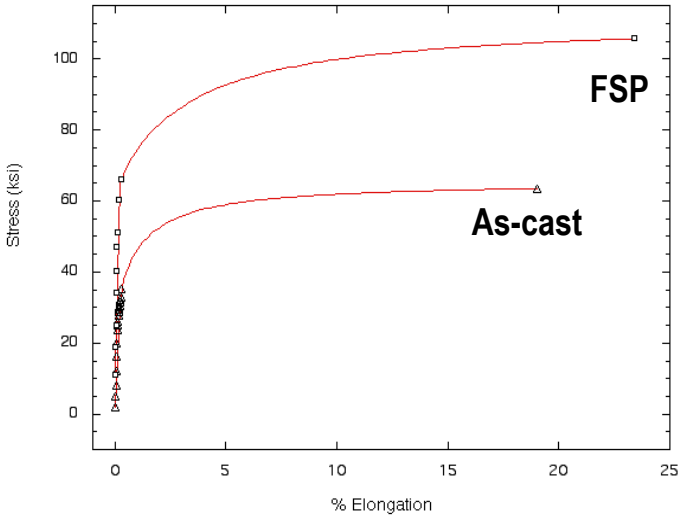

Yield Strength (ksi)		Tensile Strength (ksi)
FSP	62.8	107.8
As-cast	31.2	64.8

Figure 2.7a: Stress vs strain plot for FSP vs as-cast NAB tensile samples (data and graph courtesy of M. Mahoney). Note significant increases in tensile and yield strengths, as well as ductility for FSP'd NAB.

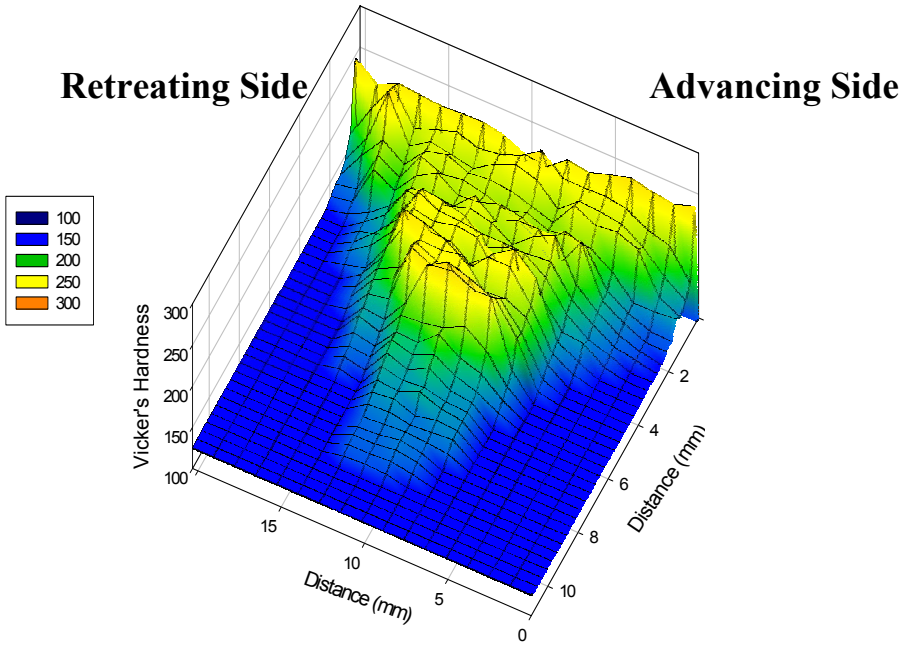

Figure 2.7b: Hardness variation in friction-stir processed NAB. Note large hardness increase in stir zone. (*Courtesy C. Park, NPS*)

III. EXPERIMENTAL PROCEDURE

This thesis evolved from a study of rolling of NAB over a wide range of temperatures to a study of fracture mechanisms in the rolling of NAB over a smaller temperature range, but including isothermal deformation of NAB during channel die compression and isothermal annealing studies.

A. SAMPLES

The samples for all of the experiments conducted during the course of this research were fabricated from a section of as-cast NAB from a large casting that was provided by NSWC Carderock. The section was approximately 25 kg in weight, and 300 mm square by 50 mm in thickness. Machining of all samples for subsequent examination was accomplished at the School.

B. ROLLING

Isothermal rolling was undertaken in order to examine the effect on microstructure of the straining associated with FSP. Based upon the results of Cuevas' [Ref. 7] work, wherein attempts to roll NAB at ambient temperature resulted in extensive cracking for all rolling schedules attempted, it was determined to start at a temperature well above room temperature. Cuevas [Ref. 7] work had that the NAB material failed catastrophically due to 'alligator' cracking during either the initial or second rolling pass. This was observed on materials in both the as cast condition as well as material that had been annealed at temperatures up to 800°C (0.85 T_m) with the same resultant fracturing.

The goal in this was to produce deformed samples for microscopy evaluation following rolling up to reductions of 10:1, or an approximate true strain of 3. This was to be accomplished using multiple passes involving reduction schedules of either 0.1 or 0.2 true strain per pass, with reheating in between passes.

Rolling billets were machined to have nominal dimensions of 32 mm in the transverse direction (TD), 19 mm in thickness along the normal (ND) direction, and 102 mm in length along the rolling direction (RD). Rolling was to be conducted at several temperatures from about 300°C up to about 850°C (just above the eutectoid temperature).

A NEY 2-160 Series II furnace was located a short distance from the FENN laboratory rolling mill to facilitate rapid transfer and rolling of the billet with minimal temperature loss. The furnace temperature was controlled with the installed thermocouple. A steel block larger in size than the rolling billets was placed on the furnace hearth to act as a heat sink and a second thermocouple was installed in a hole that had been drilled into the block. The billet temperature was typically 15°C higher than the set point of the furnace.

Rolling experiments were conducted by placing billets into the furnace and preheating for a minimum of 30 minutes to equilibrate at the rolling temperature. The rolling temperatures were expected to range from about ~400ºC (0.5 T_{melt}) up to ~800ºC (0.8 T_{melt}). Following equilibration, the samples were transferred to the rolling mill and subjected to a rolling pass in less than five seconds. The rolls were set to achieve initial reductions of either 0.1 or 0.2; sample thickness was monitored during rolling and the rolls were manually reset to maintain the initial strain per pass on subsequent passes. The effective strain rates for the rolling were approximately 1 s^{-1}. For all rolling experiments attempted at temperatures up to ~650ºC, samples failed by alligator cracking on the second or third rolling pass, and the failures became progressive more severe as temperature was increased. Up to the point of failure the samples exhibited a tendency on the lateral surfaces to 'barrel' outward, suggesting sufficient strain per pass to deform the material through its thickness. For this reason, attempts to roll at temperatures above 650ºC were abandoned.

C. CHANNEL DIE COMPRESSION

After the failure to attain the strain values desired during rolling channel die compression experiments were conducted. This is a process involving a relatively small sample (compared to those used in the rolling procedures) deformed in compression while constrained in the channel of a specially designed tool (shown in Figure 3.1). Channel die compression results in plane strain deformation and thus approximates the idealize strain state encountered during rolling. This process was accomplished using the INSTRON 4507 material testing machine with an Applied Testing System, inc. Series 3210 tubular furnace to maintain isothermal conditions.

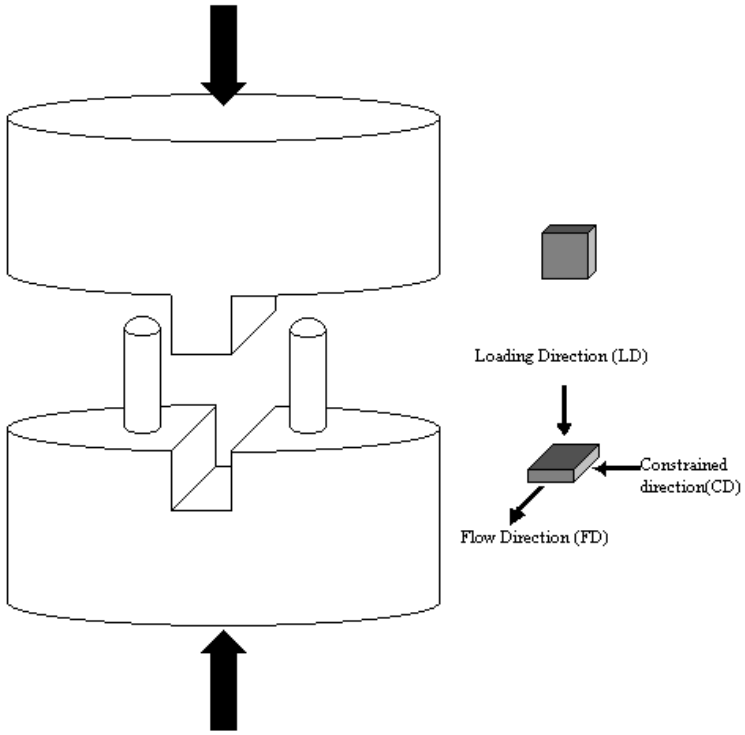

Figure 3.1: Schematic of Channel Die Compression tool. Sample depicting flow direction (FD), loading direction (LD) and constrained direction (CD) is included.

In order to conduct channel die compression the INSTRON testing machine was reconfigured from tensile testing mode to enable compression testing. A 200 kN load cell was installed and two cylindrical compression push rods were installed on the top and bottom cross heads of the machine. The basic set-up is depicted in Figure 3.2. A compression test sample that fit snugly into the die channel would be put in place with lubricant and the channel die assembly was then placed atop the lower push rod. The furnace was closed around the sample and equilibrated prior to each test.

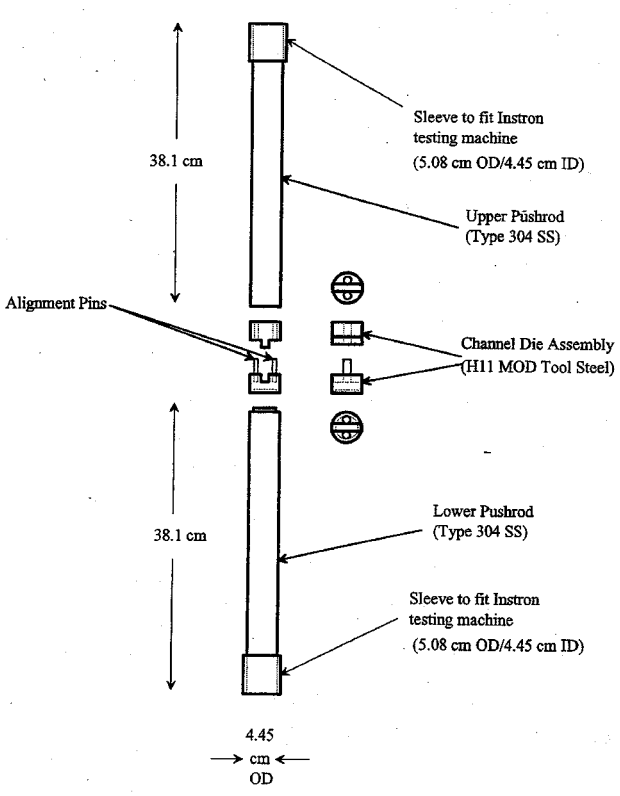

Figure 3.2: Schematic of the channel die compression set-up for the INSTRON testing machine. The channel die tool is seen in the middle. (Ref. 24)

Time constraints limited the channel die compression study to a single temperature. Three runs were conducted at 500°C to reduction ratios increasing from about 2:3 and to 3:1 (33-66% reduction). To complete these runs a clamshell design tubular furnace was utilized for temperature control. Samples were machined to dimensions to fit within the channel die tool; the most important dimension was, of course, the channel width of 8.2 mm (0.325 in). The initial dimensions of the three samples were nominally 10.3 mm (0.408 in) x 7.3 mm (0.289 in) x 8.2 mm (0.325 in). These samples and the channel die tool itself were treated with a Moly-graph multipurpose lubricant in order to minimize the sticking of the test coupon to the channel die.

While the first couple of "practice" runs (450°C and 484°C) were conducted using the INSTRON 4507 with the imbedded Series IX Automated Materials Testing System (Version 5.28) computer control and data collection abilities, the three runs

pertinent to this thesis were conducted using only the manual displacement control while monitoring of the maximum load on the load cell. The max load encountered was to be maintained at than 60 kN (12,000 lbs.) to preclude either channel die failure or load cell damage

D. ANNEALING

An annealing study was undertaken in order to record the microstructural evolution of NAB increasing temperature and time. The full run of annealing study was designed to encompass the temperatures that have been calculated as the peak temperatures attained during FSP. Samples were annealed over a range of temperatures from 380°C (~0.5 T_m) to 950°C (~0.9 T_m) and at durations of six minutes, 30 minutes, and one hour at each temperature. The sample were heated in the same furnace as the rolling samples and quenched into a large container of room temperature water in order to attain rapid cooling rates. The cooling rate was estimated as about 800°C s^{-1}. The quenching was intended to preserve elevated temperature microstructures insofar as possible.

E. SAMPLE PREPARATION (POST TREATMENT)

All of the samples were prepared by the following procedure:

1) Sectioning
2) Polishing
3) Etching
4) Microscopy

1. Sectioning

All of the samples were sectioned using a Buehler saw with a Diamond wafering blade. Speed was set relatively low at 800 rpm to ensure that the samples didn't undergo any further microstructural change due to frictional heating during sectioning. The

samples for the annealing study were all roughly the same size of 15 mm (0.6 in) x 12.5 mm (0.5 in) x 8.4 mm (0.33). The annealed samples were sectioned in half while the rolling samples and channel die compression samples were sectioned in a particular fashion.

The rolling billets were first sectioned transversely to remove the end that exhibited alligator cracking, at least 12 or 13 mm beyond the maximum extent of the cracking. The samples were then sectioned along the rolling direction in order to observe the crack profile. The Channel Die Compression samples were sectioned to reveal the LD FD plane at the midpoint of the CD axis (Figure 3.1). A lettering scheme was devised to avoid sample mix-up. This is summarized in tabular form below. Both halves of sectioned samples were scribed with the corresponding letter.

	Annealing	Rolling	Channel Die (500°C)
A	380 - 1 hr	400	3:2 reduction
B	380 - 30 min	500	2:1 reduction
C	380 - 6 min	600	3:1 reduction
D	510 - 1 hr		
E	510 - 30 min		
F	510 - 6 min		
G	600 - 1 hr		
H	600 - 30 min		
I	600 - 6 min		
J	640 - 1 hr		
K	640 - 30 min		
L	640 - 6 min		
M	770 - 1 hr		
N	770 - 30 min		
O	770 - 6 min		
P	900 - 1 hr		
Q	900 - 30 min		
R	900 - 6 min		
S	950 - 1 hr		
T	950 - 30 min		
U	950 - 6 min		

2. Polishing

Conventional grinding, polishing and etching steps were employed to prepare samples for optical microscopy. The particulate phases in NAB may be pulled out of the matrix during polishing. The following scheme was developed. Polishing was conducted on Silicon carbide (SiC) paper using water to serve as a lubricant and also to dissipate heat and the particulates of polishing. Mechanical grinding was conducted on progressively finer grit SiC papers from 500 to 4000. The procedure for each level of grit was essentially the same – the sample was first placed on the rotating polishing wheel with a moderate amount of force applied; after every 30 seconds the samples were turned 90°. This back and forth procedure was continued for about five minutes with the final few passes completed with very little force applied so that the sample apparently hydroplaned over the paper. After each grindinging step the samples were washed off with ethanol and checked to ensure that all marks were unidirectional and that no major (deep) markings remained. The final two levels of polishing utilized a Metadi Diamond Suspension as the polishing agent with grits of 0.1 and 0.05 μm.

3. Etching

Etching of the samples was conducted in order to create contrast between adjacent grains/structures. The etchant used in this experiment was suggested by the metallographers at NSWC Carderock. A 10% Ammonium-persulfate solution was used.

Following the last step of polishing the samples were subjected to a droplet of the 10% Ammonium-Persulfate solution for 10 seconds. The etchant was washed off the sample using Ethanol.

4. Miscroscopy

All samples were examined using optical microscopy techniques. The Zeiss JENOPHOT 2000 inverted light microscope with the installed digital camera and associated SEMICAPS digital imaging software provided the micrographs. A calibrated micron bar was included in each picture to better evaluate the microstructural evolution

during the various treatments. All micrographs were obtained using the 1x additional magnification lens of the microscope.

The channel die compression sample that had experienced the maximum 3:1 reduction (true strain of ~1.1) was also further examined using the TOPCON SM-510 Scanning Electron Microscope (SEM) with the Orientation Imaging Microscopy (OIM) hardware and TEXSEM software. The SEM/OIM was used to show the resultant texture and orientations of grains within the deformed sample. Images were produced using the procedures set forth in Ref. 20 & 21.

IV. RESULTS AND DISCUSSION

In this chapter the results of the experiments and the associated micrographs will be presented and explained. The objective was to correlate all of the results over a large range of temperatures in an attempt to interpret the separate effects of deformation and heating characteristic of FSP.

A. ROLLING STUDY RESULTS

In the rolling experiment the initial goal was to deform a NAB billet to a large strain by conducting several passes of the material through the rolling mill at elevated temperature.

The first run was conducted with a sample preheated to about 400°C. It, as would become the theme for these runs, was rolled successfully through two passes at 0.1 strain per pass, but then failed during the third pass. Figure 4.1(a) depicts the cracking of this sample. This cracking can be attributed to a build-up of through thickness tension or stress caused by friction between the sample and the roller. If there is any metallurgical weakness along the centerline of the slab, fracture (alligator cracking) may occur (Ref. 25).

Successive runs were conducted at temperatures up to 650°C and the strain per pass was increased to 0.2. The increase in strain per pass was in an attempt to assure through-thickness straining and avoid the build up of through-thickness stresses. All such attempts failed as well, without any notable increase in ductility with increasing temperature. In fact, the 650°C sample (Figure 4.1(b), bottom) was clearly the most catastrophic failure of all of the attempts.

Samples were chosen from the set of failed billets representing temperatures of 400°C, 500°C and 600°C and a 0.2 reduction per pass, in each case where failure had occurred after two passes. The samples were prepared as detailed in the Procedures chapter. In all cases cracking progressed through the lamellar $\alpha + \kappa_{iii}$ eutectoid constituent

in the microstructure; this may be seen in Figures 4.2 – 4.5. Data in the literature (Figures 4.6 and 4.7) suggests that ductility increases with temperature and that NAB should be sufficiently ductile to sustain large rolling strains at 650ºC. Nevertheless, catastrophic failures were still encountered at this temperature an further attempts at rolling were abandoned.


a


b

Figure 4.1(a & b): Rolling failures. Left – a 600°C rolling sample shown with an unaltered sample. Right – More examples depicting the difficulties of rolling NAB (400, 500, 650°C).

400°C

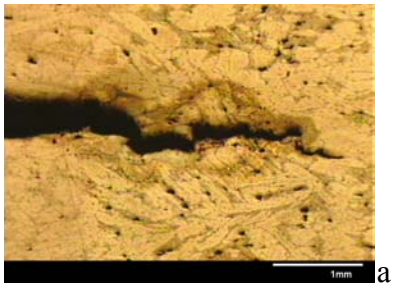

a

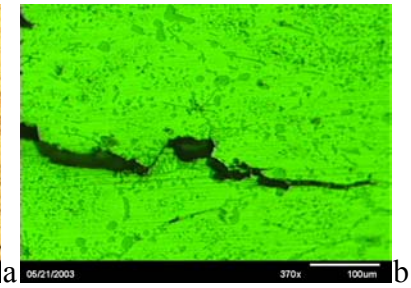

b

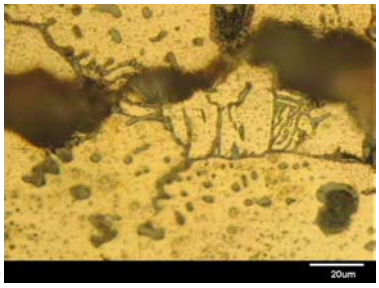

c

Figure 4.2 (a, b & c): 400°C rolling sample – magnification increasing from left to right (370x, 750x & 1500x). Evidence of a wandering crack path is easily seen in this sample.

500°C

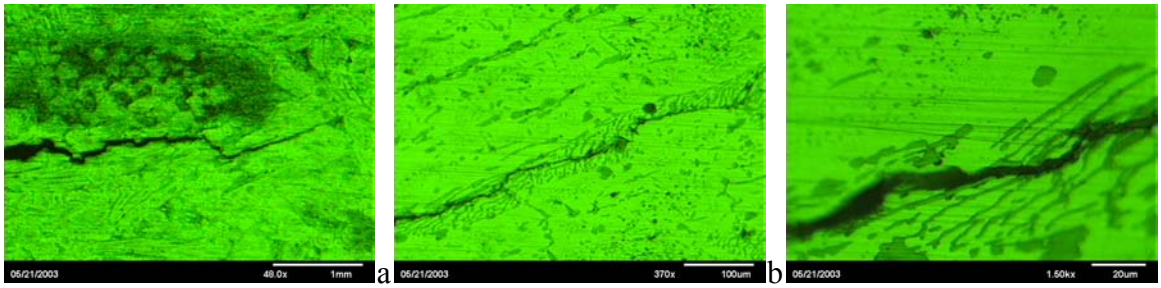

a b

c

Figure 4.3 (a, b & c): 500°C rolling sample – magnification increasing from left to right (370x, 750x & 1500x). The 750x micrograph clearly illustrates the crack's apparent tendency to propagate along the lamellar α + κ iii structure.

600°C

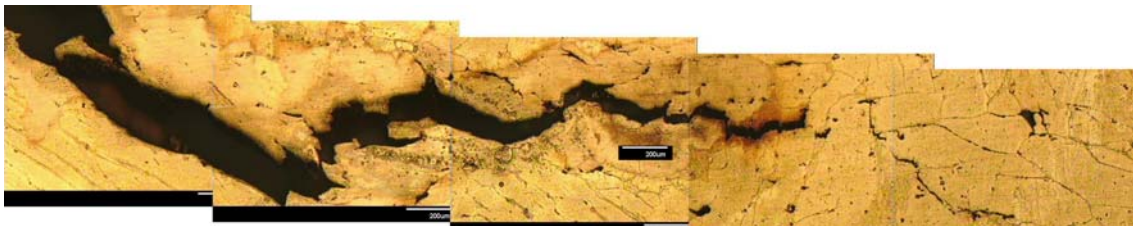

Figure 4.4: 600°C rolling sample – a micrographic montage of the crack path at 270x magnification.

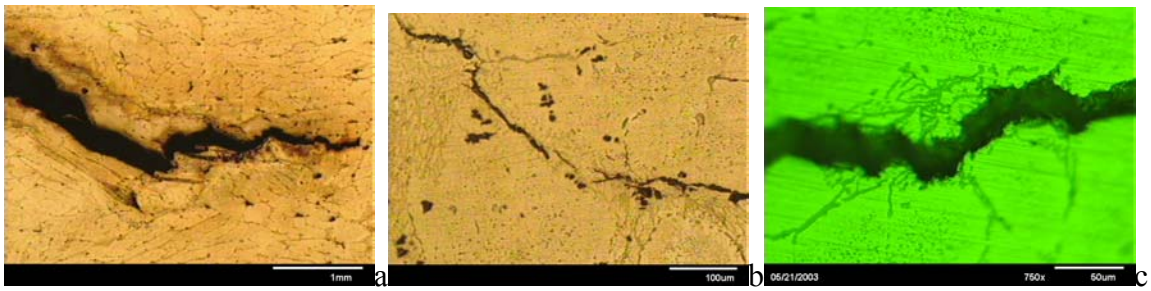

a b c

Figure 4.5 (a, b & c): 600°C rolling sample – magnification increasing from right to left (370x, 750x & 1500x). Again the crack's tendency to follow the lamellar structure is seen in the 750x micrograph.

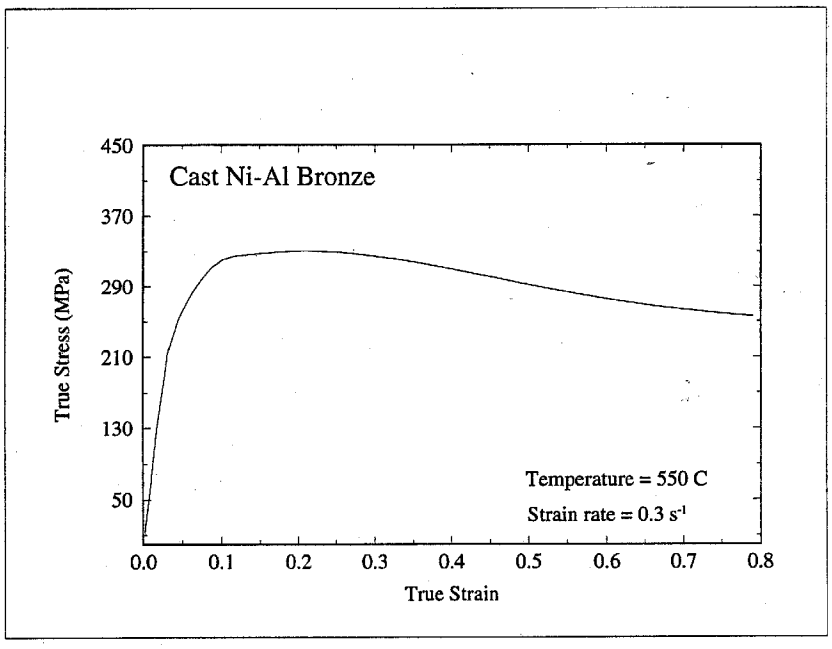

Figure 4.6: Representative Stress vs. Strain curve for NAB. [Ref. 26]

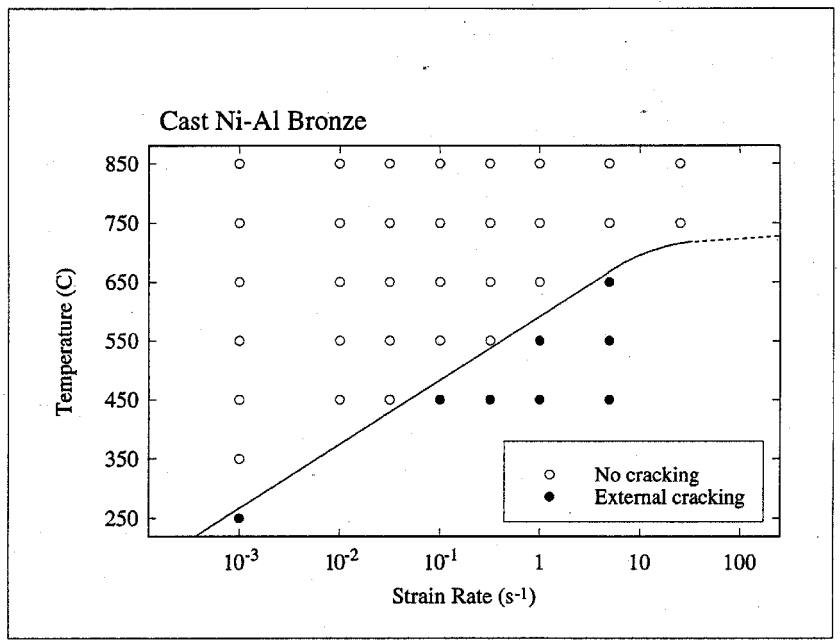

Figure 4.7: External Cracking diagram. [Ref. 26]

B. CHANNEL DIE COMPRESSION RESULTS

The channel die compression testing was able to attain much larger strains than attained in the rolling studies at a similar temperature. The reduction of strain rate and the introduction of a plane strain condition without through-thickness tension due to friction with the rolls are likely responsible for this result. In channel die compression the channel constrains the sample and leads to plane strain compression.

Figure 4.8 shows the samples for the three successful 500°C channel die compression tests. The subsequent micrographs (Figures 4.9-11) were acquired after deformation. These micrographs demonstrate that NAB can be deformed at moderate temperature within the range attempted in the rolling studies. The channel's constraining effect upon the sample and the lack of the through thickness tension gradient seen in rolling creates a strain state which is conducive to large amounts of deformation. After a small strain of ~0.3 there is little apparent effect on the microstructure. At a larger strain, the lamellar $\alpha + \kappa_{iii}$ constituent appears to experience deformation along with the matrix; in fact, the lamella appear to have experienced buckling without fracture in Fig. 4.10c. At a still greater strain (1.1) the lamellar structure appears to be breaking up into a particulate distribution. OIM results suggest that the material remains coarse grained; there is only one orientation evident in the pole figures in Fig. 4.12.

Figure 4.8: Channel Die Compression samples with original sample. This picture shows the finished products from the three 500°C runs set next to an undeformed sample. The three deformed samples are arranged from top to bottom in increasing degree of strain

input.

Sample	CD	FD	LD	reduction	Strain
Control	8.2	7.3	0.408	0%	0
A	8.2	14	5.8	44%	0.574
B	8.2	16.9	4.5	56%	0.828
C	8.2	23.3	3.4	67%	1.11

Table 2. Results of the Channel Die Compression experiments. All three samples were tested at 500°C.

below: sample A – 370x, 750x & 1500x


a

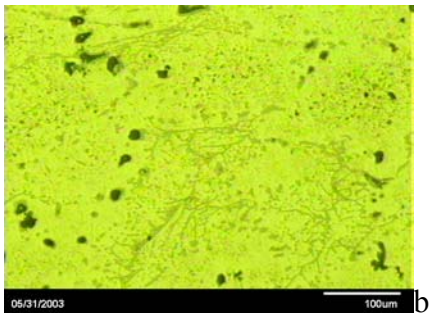

b

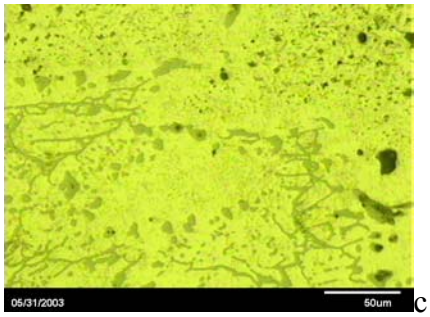

c

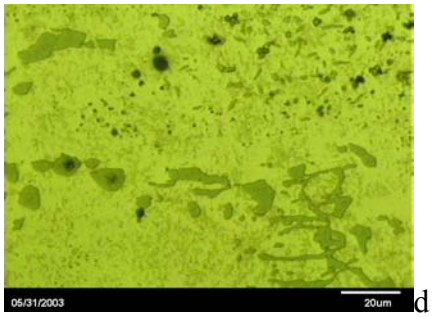

d

Figure 4.9 (a, b, c & d): Sample A - 500°C deformed to approximately a 3:2 reduction ratio: a – deformed sample next to original. b, c & d – 370x, 750x & 1500x , respectively.


a
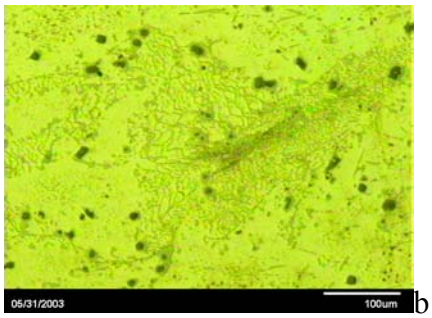

b
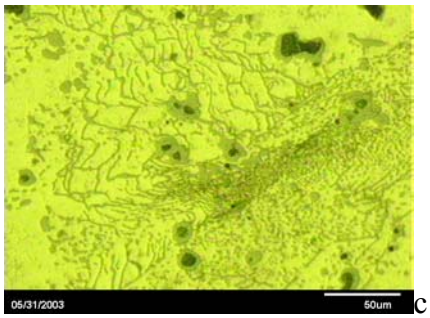

c
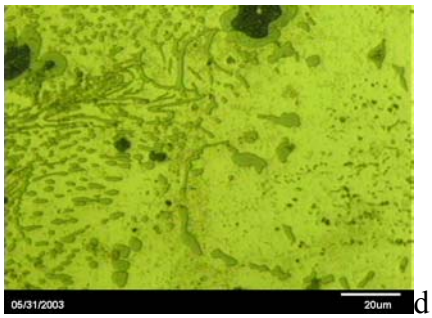

d

Figure 4.10 (a, b, c & d):): Sample B - 500°C deformed to approximately a 2:1 reduction ratio: a – deformed sample next to original. b, c & d – 370x, 750x & 1500x , respectively.


a


b
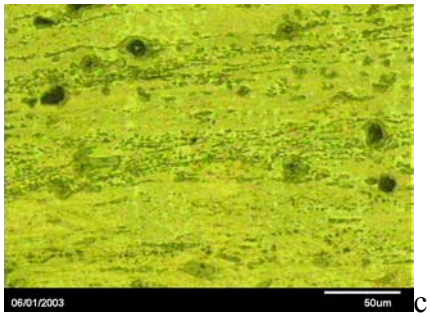

c
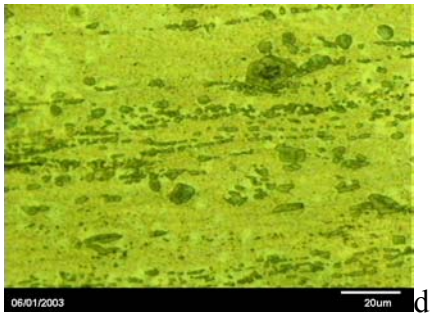

d

Figure 4.11 (a, b, c & d):): Sample C - 500°C deformed to approximately a 3:1 reduction ratio: a – deformed sample next to original. b, c & d – 370x, 750x & 1500x , respectively.

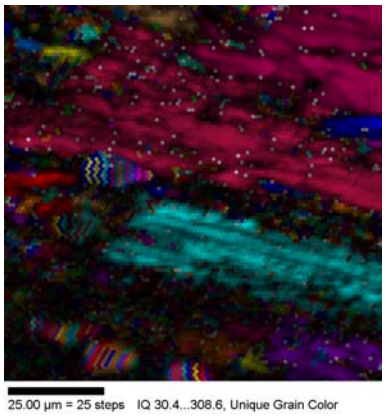

a

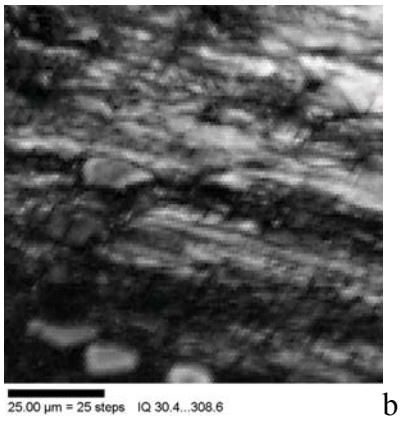

b

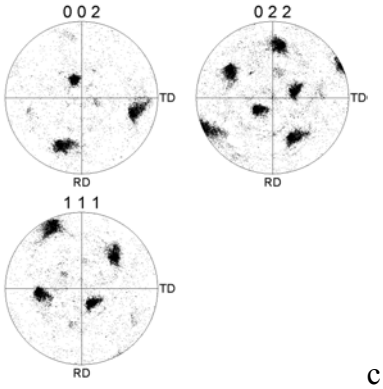

c

Figure 4.12 (a, b & c): Scanning Electron Microscope results from Channel Die Compression sample C (reduction ratio 3:1). a & b are micrographs of the resultant deformed structure at a magnification of approximately 250x. The three pole figures that were calculated for this scan location are represented in c. These pole figures are most probably representative of a copper based structure.

C. ANNEALING RESULTS

The annealing study examined microstructures over a wider range of temperatures for this material. Little change from the as-cast microstructure is observed for the lowest four temperatures investigate: 380ºC, 510ºC, 640ºC, and 770ºC (Figures 4.13-4.16) – all of these temperatures are below the eutectoid (approximately 800ºC). Upon heating to 900°C, even at a short duration as 6 minutes (Figure 4.19), grain coarsening and the results of transformation of the lamellar $\alpha + \kappa_{iii} \rightarrow \beta$ above 800ºC are evident. While the phase diagram (Figure 2.3) does not show the eutectoid explicitly, the dissolution of the

lamellar structure is clear. The large darker areas are the β formed during annealing and then transformed to a fine Widmanstäten α, or banitic or martensitic β'. This temperature range corresponds to anticipated temperatures in the stir zone. At 900°C an increase in duration of the soak results in greater amounts of retransformation to β and a consequent increase in the volume fraction of β transformation products under the quenching conditions employed. This also suggests that dwell time at temperature during FSP will be a factor in the extent of transformation during FSP. The 950°C sample also shows the same retransformation of the lamellar structure with the corresponding appearance of the β transformation products under the quenching conditions.

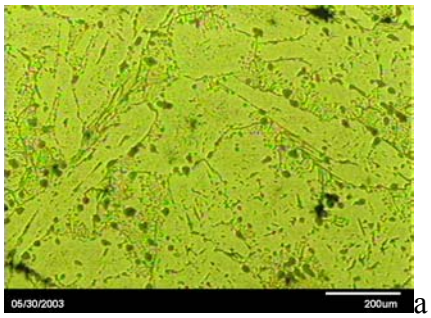

a

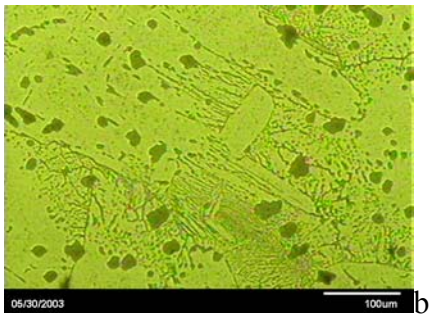

b

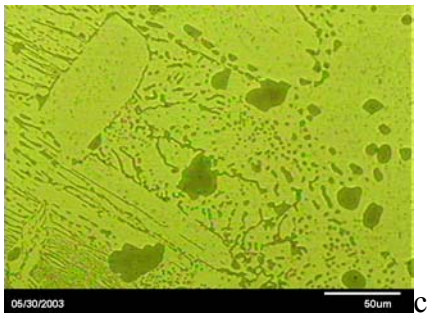

c

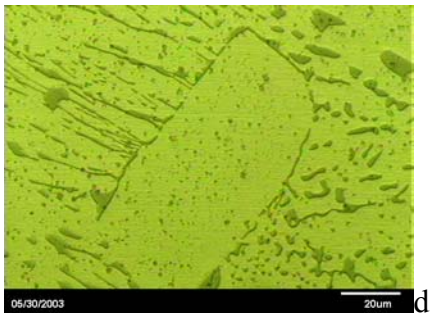

d

Figure 4.13 (a, b, c & d) – Annealing sample micrographs – Sample A – 380°C, 1 hr (290x, 370x, 750x and 1500x, respectively). All phases are present with little or no sign of temperature affect.

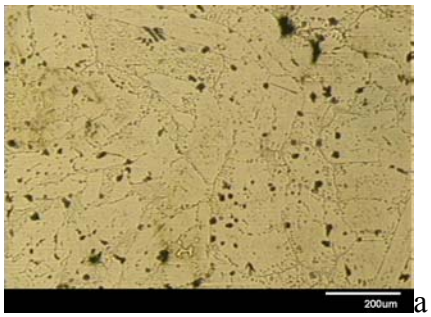

a

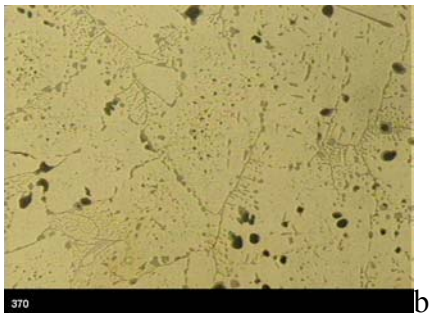

b

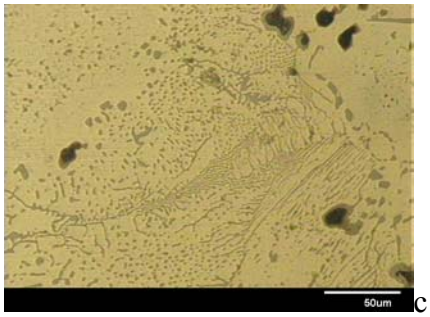

c

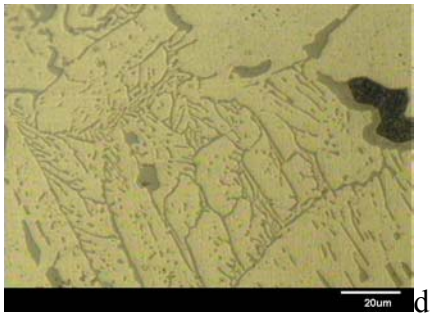

d

Figure 4.14 (a, b, c & d) – Annealing sample micrographs – Sample D – 510°C, 1 hr (290x, 370x, 750x and 1500x, respectively). Some grain coarsening is evident.

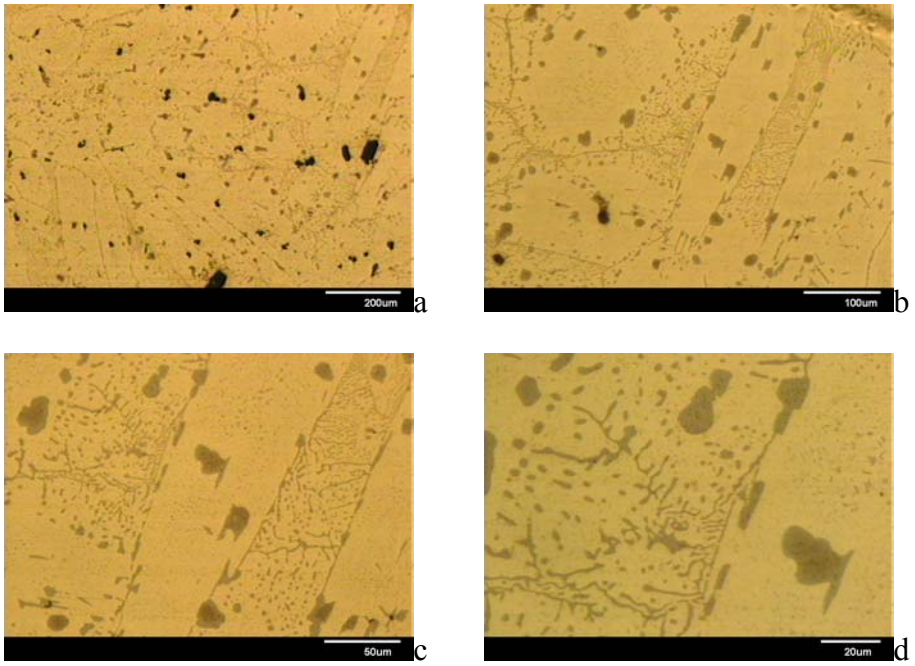

Figure 4.15 (a, b, c & d) – Annealing sample micrographs – Sample J – 640°C, 1 hr (290x, 370x, 750x and 1500x, respectively). All phases are present with little or no sign of temperature affect.

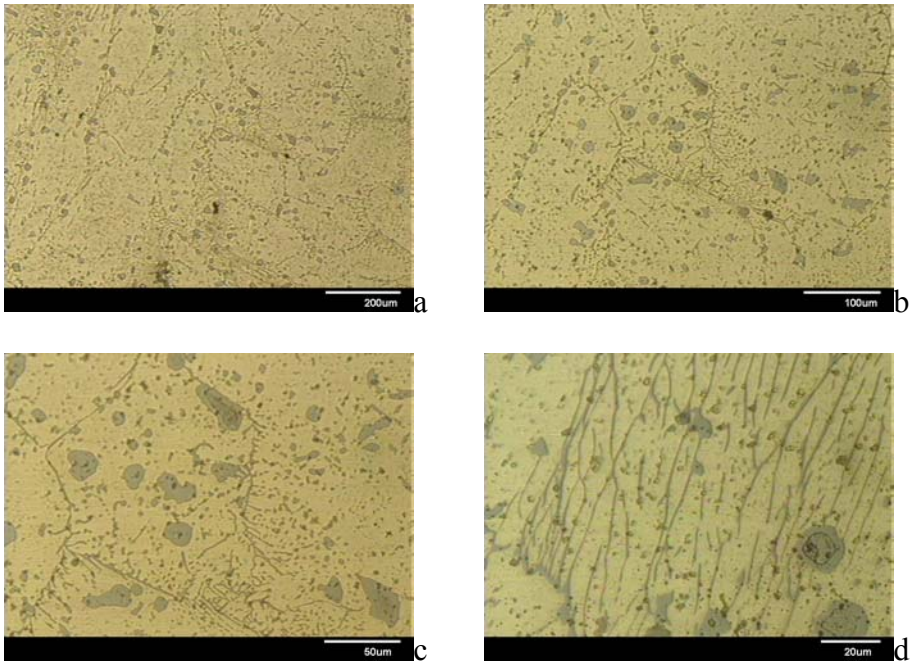

Figure 4.16 (a, b, c & d) – Annealing sample micrographs – Sample O – 770°C, 6 minutes (290x, 370x, 750x and 1500x, respectively). All phases are present with little or no sign of temperature affect.

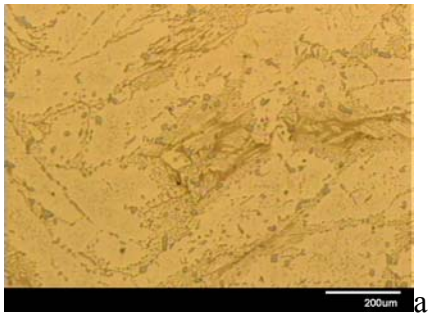

a
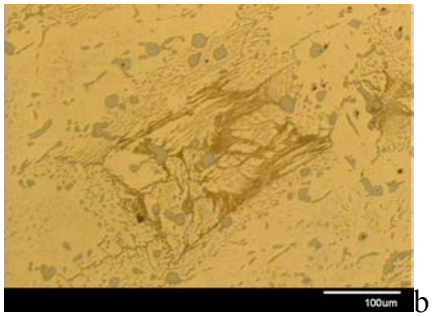

b
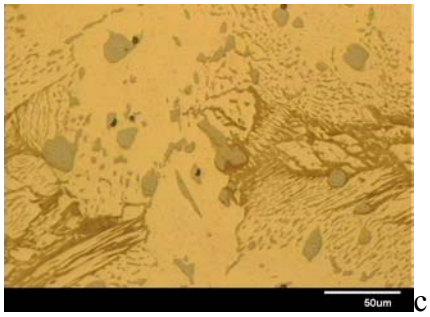

c
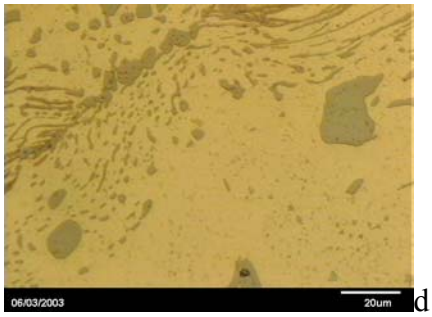

d

Figure 4.17 (a, b, c & d) – Annealing sample micrographs – Sample N – 770°C, 30 minutes (290x, 370x, 750x and 1500x, respectively). All phases are present with little or no sign of temperature affect.

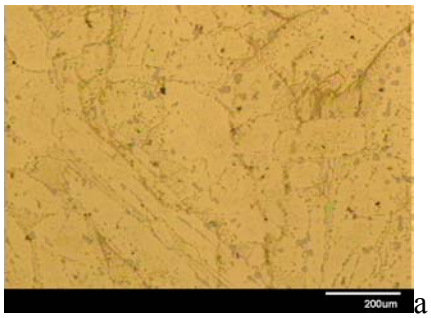

a
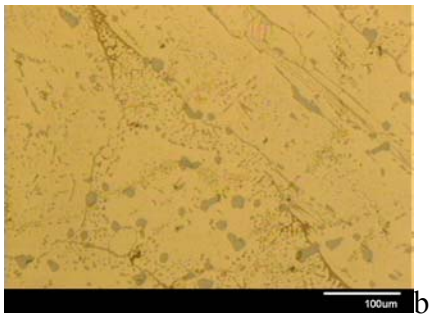

b
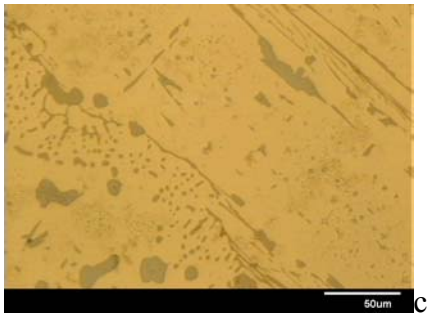

c


d

Figure 4.18 (a, b, c & d) – Annealing sample micrographs – Sample M – 770°C, 1 hr (290x, 370x, 750x and 1500x, respectively). All phases are present with some signs of temperature affect seen in the lamellar structure's coarsening.

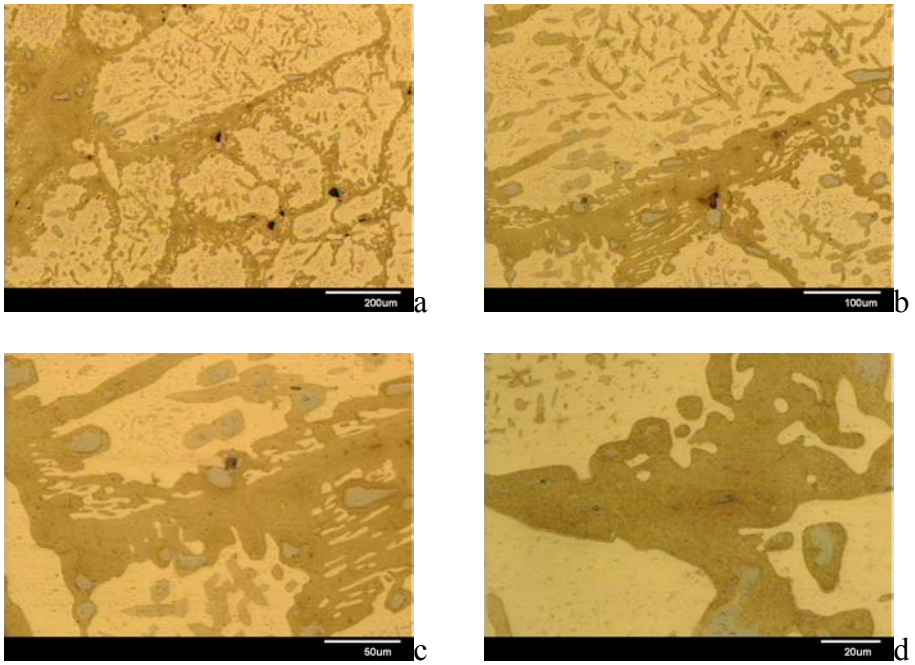

Figure 4.19 (a, b, c & d) – Annealing sample micrographs – Sample R – 900°C, 6 minutes (290x, 370x, 750x and 1500x, respectively). The lamellar structure is retransforming into β form.

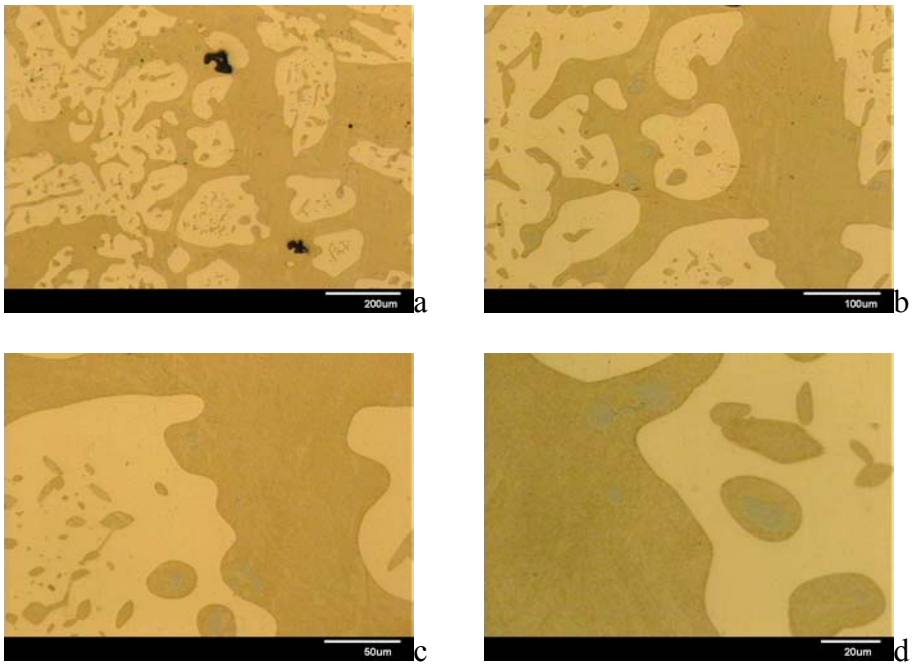

Figure 4.20 (a, b, c & d) – Annealing sample micrographs – Sample P – 900°C, 1 hr (290x, 370x, 750x and 1500x, respectively). The β regions have increased in size with time.

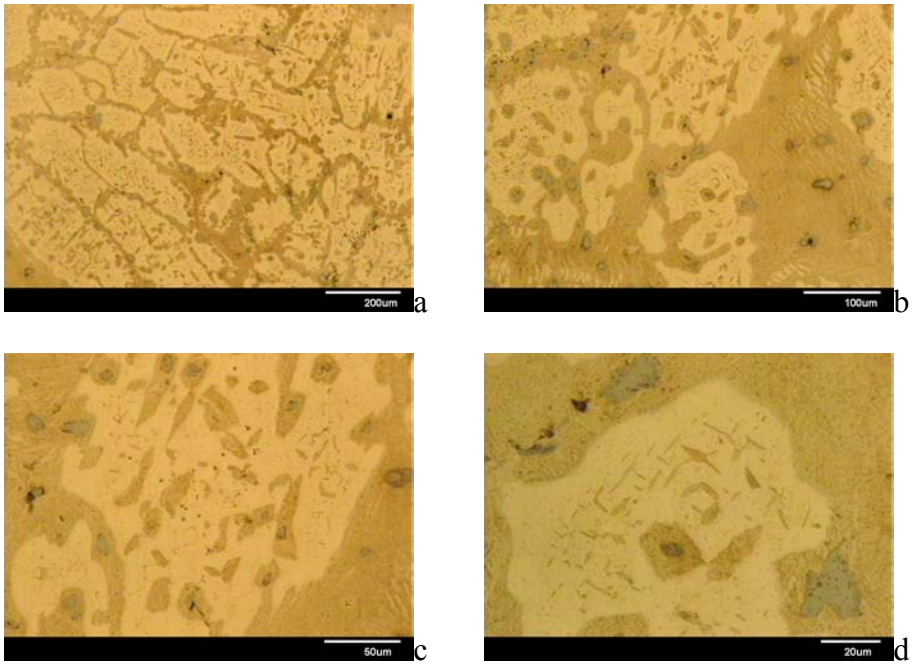

Figure 4.21 (a, b, c & d) – Annealing sample micrographs – Sample U – 950°C, 6 minutes (290x, 370x, 750x and 1500x, respectively). Retransformation of the lamellar structure is evident.

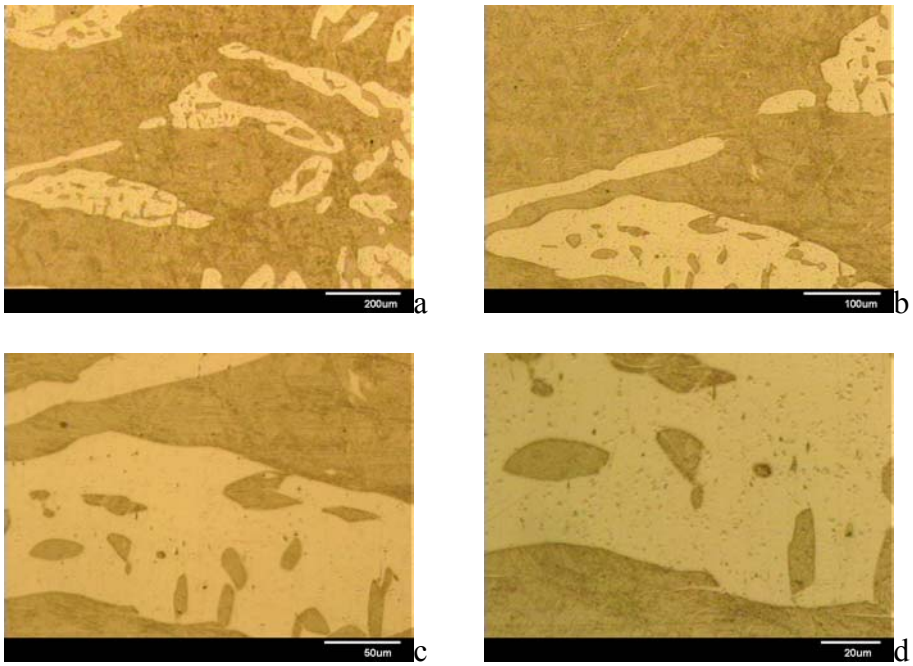

Figure 4.22 (a, b, c & d) – Annealing sample micrographs – Sample S – 950°C, 1 hr (290x, 370x, 750x and 1500x, respectively). As expected from the 900 degree set, this set of micrographs shows a retransformation of the particulate forms to the β form.

The limited ductility of the lamellar structure and its role in the failure of the rolling billets suggests that rolling may be feasible above the eutectoid temperature. The deformation of the lamellar $\alpha + \kappa_{iii}$ constituent during channel die compression suggests that deformation of this constituent in the TMAZ may occur as long as the strain state does not result in local tension.

D. NEED FOR FOLLOW-ON WORK

This investigation has indicated that further study of conventional deformation mechanisms and annealing treatments will benefit the understanding of FSP. Further rolling studies should utilize temperatures above the euctectoid (> 800°C) to determine the effect of the transformation of the lamellar $\alpha + \kappa_{III}$ structure into β upon the rolling characteristics of NAB.

As with the rolling study, the channel die compression study may be expanded to include the eutectoid temperature range and greater strain states (within tool and testing machine limits). Further testing using the channel die followed by mapping the resultant microstructures would most likely be a more probable next step than a furthering of the rolling studies. Finally, a more refined annealing schedule within the eutectoid region would be beneficial.

THIS PAGE INTENTIONALLY LEFT BLANK

LIST OF REFERENCES

1. Duma, J.A., "Heat Treatments For Optimizing Mechanical and Corrosion Resisting Properties of Nickel-Aluminum Bronzes," *Naval Engineers Journal*, v. 87, p. 45-64, 1975.

2. Metals Handbook, 9th Ed., v. 2, Properties & Selections: Nonferrous Alloys and Pure Metals.

3. Military Specifications For Bronze, Nickel-Aluminum (UNS C95800), Castings For Seawater Service (MIL-B-24480A), 20 June 1985.

4. American Society for Testing and Materials (ASTM) B148 – 93a, Standard Specification for Aluminum-Bronze Sand Castings.

5. Sahoo, M., "Structure and Mechanical Properties of Slow-Cooled Nickel-Aluminum Bronze Alloy C95800," *AFS Trans*, v. 90, p. 913-926, 1982.

6. Culpan, E.A. and Rose, G., "Corrosion Behaviour of Cast Nickel Aluminium Bronze in Sea Water," *British Corrosion Journal,* v. 14, p. 160-166, 1979.

7. A.M. Cuevas, MS Thesis, "Microstructure Characterization of Friction-Stir Processed Nickel-Aluminum Bronze through Orientation Imaging Microscopy," Naval Postgraduate School, Monterey, CA, 2002.

8. W.M. Thomas, E.D. Nicholas, J.C. Needham, M.G. Murch, P. Templesmith and C.J. Dawes, "Friction Stir Butt Welding," G.B. Patent Application No. 9125978.8, Dec. 1991; U.S. Patent No. 5460317, Oct. 1995.

9. Mishra, R.S. and Mahoney, M.W., "Friction Stir Processing: A New Grain Refinement Technique to Achieve High Strain Rate Superplasticity in Commercial Alloys," *Materials Science Forum,* v. 357-359, p. 507-514, 2001.

10. P.B. Berbon, W.H. Bingel, R.S. Mishra, C.C. Bampton and M.W. Mahoney, "Friction Stir Processing: A Tool to Homogenize Nanocomposite Aluminum Alloys," *Scripta*

Materialia, v. 44, p. 61-66, 2001.

11. R.S. Mishra, M.W. Mahoney, S.X. McFadden, N.A. Mara and A.K. Mukherjee, "High Strain Rate Superplasticity In A Friction Stir Processed 7075 Al Alloy," *Scripta Materialia*, v. 42, p. 163-168, 2000.

12. Weston, G.M., "Survey of Nickel-Aluminium-Bronze Casting Alloys on Marine Applications," Australia Dept. of Defence Report, DSTO MRL, Melbourne, Victoria, MRL-R-807, 1981.

13. Weill-Couly, P. and Arnaud D., "Influence De La Composition Et De La Structure Des Cupro-Aluminiums Sur Leur Comportment En Service," *Fonderie*, no. 322, p. 123-135, 1973.

14. Culpan, E.A. and Rose, G., "Microstructural Characterization Of Cast Nickel Aluminium Bronze," *Journal of Materials Science*, v. 13, p. 1647-1657, 1978.

15. F. Hasan, A. Jahanafrooz, G.W. Lorimer and N. Ridley, "The Morphology, Crystallography, and Chemistry of Phases in As-Cast Nickel-Aluminum Bronze," *Met. Trans A*, v. 13a, p.1337-1345, 1982.

16. A. Jahanafrooz, F. Hasan, G.W. Lorimer and N. Ridley, "Microstructural Development in Complex Nickel-Aluminum Bronze," *Met. Trans A*, v. 14a, p. 1951-1956, 1983.

17. D.E. Bell, MS Thesis, "Microstructural Development and Corrosion Resistance of Laser-Welded Nickel-Aluminum Bronze," Pennsylvania State University, PA, 1994.

18. Private communications, M.W. Mahoney, Rockwell Science Center, Thousand Oaks, CA, November 2002.

20. G.R. Canova, U.F. Kocks and J.J. Jonas, "Theory of Torsion Texture Development," *Acta Metall.*, v. 32, p. 211-226, 1984.

21. Brezina, P, "Heat Treatment of Complex Aluminum Bronzes," *Int. Met. Rev*., v. 27, n. 2, p. 77-120, 1982.

22. Orientation Imaging Microscopy (OIM) Data Collection User Manual, ver. 1.0, TexSEM Laboratories, Inc., 1998.

23. Orientation Imaging Microscopy (OIM) Analysis, ver. 3.0, TexSEM Laboratories, Inc., 2000.

24. M.A. Ballou, MS Thesis: "The Effect of Thermomechanical Processing on the Tensile Properties and Microstructure of a 6061 Al-Al_2O_3 Metal Matrix Composite." Naval Postgraduate School, Monterey, CA, 1995

25. G.E. Dieter "Mechanical Metallurgy" 3rd Edition. p. 605.

26. National Center for Excellence in Metalworking Technology: Atlas of Formability – Cast Ni-Al Bronze, 1995

27. A. Askari, Boeing INC., Private Communication, June 2003.

THIS PAGE INTENTIONALLY LEFT BLANK

INITIAL DISTRIBUTION LIST

1. Defense Technical Information Center
   Ft. Belvoir, Virginia

2. Dudley Knox Library
   Naval Postgraduate School
   Monterey, California

3. Professor Terry McNelley
   Naval Postgraduate School, Dept. of Mechanical Engineering
   Monterey, California

4. Professor Y.W. Kwon
   Naval Postgraduate School, Dept. of Mechanical Engineering
   Monterey, California

5. CDR S. Cunningham
   Naval Postgraduate School, Dept. of Mechanical Engineering
   Monterey, California